

Facile in-situ synthesis of a zinc oxide crystals/few-layered graphene flake composite for enhanced photocatalytic performance



Weiwei Tie^{a,b}, Surjya Sarathi Bhattacharyya^c, Yanan Wang^a, Weiwei He^{a,**},
Seung Hee Lee^{b,*}

^a Key Laboratory of Micro-Nano Materials for Energy Storage and Conversion of Henan Province, Institute of Surface Micro and Nano Materials, College of Advanced Materials and Energy, Xuchang University, Xuchang, Henan 461000, China

^b Applied Materials Institute for BIN Convergence, Department of BIN Convergence Technology and Graduate School of Printable and Flexible Electronics, Chonbuk National University, Jeonju, Jeonbuk 561-756, South Korea

^c Asutosh College, 92, Shyamaprasad Mukherjee Road, Kolkata 700 026, West Bengal, India

ARTICLE INFO

Article history:

Received 21 February 2017

Received in revised form 11 July 2017

Accepted 1 August 2017

Available online 8 August 2017

Keywords:

Zinc oxide

Graphene flakes

In-situ solution method

Photocatalytic properties

ABSTRACT

An efficient multilayer graphene-based semiconductor catalyst of reduced graphene oxide flakes decorated with zinc oxide crystals (ZnO/RGO) has been successfully synthesized in-situ using a facile low-temperature solution procedure. Zinc acetate was used as a single precursor with dimethyl sulfoxide acting as the mixing agent. The photocatalytic materials were then characterized using scanning electron microscope and X-ray diffraction patterns, as well as Raman, FT-IR, XPS and UV–vis spectroscopies. The ZnO crystals were found covalently bonded onto reduced graphene flakes through direct Zn–O–C path, and this could allow photogenerated electrons quickly transferring from the ZnO to RGO and thereby efficiently lengthened the lifetime of the photogenerated charge carriers from the ZnO crystals. This result has been further confirmed by surface photovoltage spectrum studies. Compared to pure ZnO, small amount of 0.15 mg/ml ZnO/RGO hybrid had exhibited superior photocatalytic activity and reproducible catalytic efficiency onto 2×10^{-2} mg/ml Rhodamine B dye in consecutive uses. The detailed formation of synthesis and characterization as well as photocatalytic mechanisms have also been explored.

© 2017 Elsevier B.V. All rights reserved.

1. Introduction

ZnO nanoparticles (NPs) have been well developed as photocatalyst for effective elimination of toxic chemicals from the environment [1,2] due to their high oxidizing power, nontoxic nature, wide band gap, and high cost performance [3–6]. However, although ZnO NPs have a distinctive size as well as morphology-dependent optical and electronic properties, widely practical applications are limited by the rapid recombination of the photogenerated charge carriers as well as the system's passive photo-response toward solar spectrum light.

Recently, functionalizing carbonaceous materials with ZnO NPs have opened up new opportunities to design and develop novel photocatalytic composites [7–12]. Due to its strong optical

absorption characteristics and extremely effective electron transfer capability, graphene (GR) is a highly desirable and appropriate candidate for use as a two-dimensional (2-D) catalyst support with large surface area [8–12]. Using ZnO NPs to modify GR may also prevent restacking and agglomeration of GR during the reduction process by van der Waals interactions between GR sheets [13]. Recent studies have examined various ZnO/GR hybrid systems and have exhibited improved photocatalytic performance [10–12]. Li et al. [10] and Wu et al. [11] have utilized a hydrothermal method to synthesize ZnO/GR composites with good structural and optic catalytic properties. Neelgund et al. [12] has evaluated the effectiveness of a new hybrid of ZnO/cobalt phthalocyanine/GR constructed via chemical deposition and a subsequent reduction route using a toxicity reducing agent. ZnO/GR composites made using either surfactant or microwave-assisted synthesis methods have also exhibited brilliant photocatalytic activity for the degradation of organic dyes [14,15]. Though great progress has been made in the synthesis of ZnO/GR composites, the most frequently adopted routes for synthesis remain hydrothermal

* Corresponding author.

** Corresponding author.

E-mail addresses: heww1982@163.com (W. He), lsh1@jbnu.ac.kr, lsh1@chonbuk.ac.kr (S.H. Lee).

methods [10,11], utilizing a toxicity reducing agent [12], or surfactant or microwave-assisted methods [14,15]. Additionally, few study has been focused on reproducible catalyst for practical application. Interestingly, multilayer graphene flakes (pi-stacked few graphene sheets) as catalysts support [16], rather than single graphene, could be beneficial in consecutive uses due to their relatively high mass and poor solubility. Therefore, a simpler and more efficient method to covalently anchor ZnO NPs onto 2-D graphene flakes through direct interatomic bonding remains highly desirable for accelerating electron transfer and separate process, and reproduceable photocatalytic application of hybrid catalyst made using new method also need to be studied.

In the present work, a simple in-situ synthesis for hybrid catalyst of ZnO crystals covalently bonded few-layered graphene flakes (ZnO/RGO) has been developed which requires only a simple one-step mixing process without any reducing agents or high temperature/pressure conditions. This new method can be considered as a promising alternative to the abovementioned typical methods. Meanwhile, the effectiveness of covalent functionality of ZnO crystals onto RGO flakes through Zn–O–C linking has been evaluated by testing its ability to degrade an important dye, Rhodamine B (RhB), and its reproduceable stability in consecutive uses. The photoinduced charge transfer and separation process has been directly monitored through transient surface photovoltage. It is hoped that this hybrid catalyst, based on the effective electron transfer cascade system through covalent Zn–O–C bond, can ultimately achieve reduced recombination of photogenerated electron-hole pairs, high-speed transfer of excited electrons from the semiconductor surface, and improved catalytic reproducibility in circulation.

2. Experimental

2.1. Materials

The highly purified (> 99%) natural graphite flakes (320 mesh) used to prepare photocatalytic composites were supplied by Alfa Aesar. All analytical grade chemicals were used as received without further purification. These included Zinc acetate ($\text{ZnAc}_2 \cdot \text{H}_2\text{O}$, 98.5%), dimethyl formamide (DMF, 99%), hydrochloric acid (HCl, 37%), sulfuric acid (H_2SO_4 , 98%), phosphoric acid (H_3PO_4 , 85%), hydrogen peroxide (H_2O_2 , 30%), potassium permanganate (KMnO_4), and absolute ethanol obtained from J&K chemical technology Ltd. Deionized water was used in all experiments.

2.2. Preparation of graphite oxide

Graphite oxide was made by chemically oxidizing and exfoliating from natural graphite flakes according to an improved Hummers' method [17]. About 5.0 g of the purchased graphite flakes were combined with KMnO_4 (30.0 g) and then slowly mixed with 200 ml of a 3:1 (v/v) mixture of concentrated H_2SO_4 (98%) and H_3PO_4 (85%) placed under ice bath. The solution was placed in a 250 ml glass bottle and heated to 50 °C, and then stirred for 24 h. Next, the reaction was cooled to room temperature and poured onto ice water (200 ml) mixed with 30% H_2O_2 (10 ml). The supernatant was collected and repeatedly centrifuged following by successive washings with deionized water until solution pH reached 7. The solid product obtained from this method was finally vacuum oven-dried at 45 °C and hereafter called graphite oxide.

2.3. Preparation of ZnO/RGO composite

In order to synthesize the ZnO/RGO composite, 4 mg dried graphite oxide was dispersed in 40 ml of DMF and ultrasonicated for 30 min, during which the graphite oxide was exfoliated to form graphene oxide (GO). Next, about 0.2 g ZnAc_2 was added to the solution and then heated to 95 °C. The mixture was kept stirring for 5 h, and washed several times with distilled water and ethanol in order to remove unreacted products. The mixture was then vacuum-dried at 60 °C for 12 h to obtain the final ZnO/RGO composite. For comparison, pure ZnO was also synthesized using the same procedure but without the addition of graphite oxide. The sample of ZnO-RGO mixture was prepared by impregnation method using pure ZnO and RGO following the abovementioned same procedure. The synthesis routes used for ZnO NPs and the ZnO/RGO composite are represented in Schemes 1 and 2.

2.4. Characterization

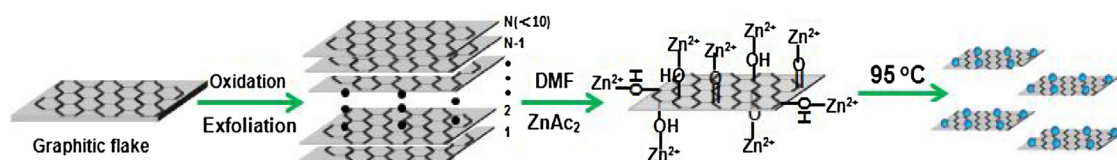
X-ray diffraction (XRD) patterns were collected using a X-ray diffractometer (Bruker D8 Advance) with $\text{Cu-K}\alpha$ radiation ($\lambda = 1.5406 \text{ \AA}$). The surface morphologies of the samples were examined using a scanning electron microscope (SEM, ZEISS EVO LS15). Raman spectroscopic analysis was performed using a Perkin Elmer Spectrum-GX and Renishaw in Via Raman spectrometer with a laser excitation of 532 nm. A UV-vis-Infrared spectrophotometer (Agilent Cary-5000) was used to record the UV-vis spectra of various samples. FT-IR spectroscopic analyses were carried out using a JASCO FT/IR-460 plus FT-IR spectrometer. A XPS spectrometer (Thermo escalab 250×1, USA) with $\text{Al-K}\alpha$ radiation ($h\nu = 1486.6 \text{ eV}$) was used to test X-ray photoelectron spectroscopy of samples. Transient surface photovoltage (TPV) spectroscopic analysis was performed following a standard method as reported by Y. Lei et al. [18]. In summary, powder samples for each other are first placed over an indium tin oxide (ITO) coated glass substrate and sandwiched between another ITO coated glass substrate. Mica spacers were used to precisely maintain the gap between the two electrodes. A third-harmonic Nd:YAG laser (Quantel Brilliant Eazy: BRILEZ/IR-10) was utilized as the source for laser pulses (355 nm and 532 nm with a pulse width of 4 ns), and TPV signals were recorded using a 500 MHz digital oscilloscope (TDS 3054C, Tektronix).

2.5. Photocatalytic activity

In order to analyze the photocatalytic performance of the samples, the degradation process of Rhodamine B in water was monitored 300 W Mercury light irradiation (XPA, China). Small amounts of powdered samples (~7.5 mg each) were dispersed into a solution of 1 mg RhB in 50 ml water. The homogeneous suspension was initially stirred in the dark for 30 min to achieve adsorption-desorption equilibrium and then irradiated for several different exposure times before being placed in a centrifuge to remove the dispersed powder. Once a sample solution was clean and transparent it was analyzed using UV/vis spectroscopy. The concentration of the RhB solution was calculated using the UV absorbance at 554 nm wavelength and used to determine their relationship with irradiation time.



Scheme 1. Schematic representation of the formation of ZnO crystals.



Scheme 2. Schematic illustration of the formation of ZnO/RGO composite.

3. Result and discussion

The formation process of pure ZnO NPs and the ZnO/RGO composite is summarized graphically in Schemes 1 and 2. Zn^{2+} ions are chemically adsorbed onto the negatively charged surfaces of GO sheets via electrostatic force [9]. The slight heating to 95°C induces the nucleation of ZnO onto the GO surface via intermolecular hydrogen bonds as well as electrostatic attraction between ZnO^{2-} and the functional groups on the GO sheets. At the same time, the in-situ formation of ZnO NPs also leads to the reduction of GO to RGO [19], thus forming the desired ZnO/RGO composite. The morphologies of pure ZnO and the ZnO/RGO hybrid were observed using SEM in order to directly analysis the structure of the ZnO crystals decorating the graphene sheets, and more specifically, investigate the influence of multilayered graphenes onto the morphology of the ZnO crystals. The SEM micrographs shown in Fig. 1a display a significant aggregation of the ZnO NPs into pure ZnO crystals with diameters of $\sim 0.8\text{--}1.0\ \mu\text{m}$. However, Fig. 1b shows that in the case of the ZnO/RGO hybrid, ZnO crystals half that size spread uniformly and tightly across the graphene flakes. This indicates that the graphene may interact with ZnO NPs to inhibit their aggregation.

X-ray diffraction (XRD) patterns were collected in order to compare the phase and structure of ZnO/RGO composites to that of pure ZnO and GO. As shown in Fig. 2, the XRD pattern of GO has a sharp peak centered on 10.8° . This feature is attributed to the (002) plane reflection of the GO carbon structure. While natural graphite has an interplanar distance ($d=002$) of only $3.35\ \text{\AA}$, the measured interplanar spacing ($d=002$) for GO is much larger at $7.1\ \text{\AA}$ due to the intercalated water molecules, hydroxyl, carbonyl, and carboxyl groups. However, when the ZnO/RGO hybrid is examined, the GO (001) diffraction peak at 10.8° has disappeared, while a new, broad characteristic peak appears at 26.2° due to the (002) plane and corresponding to an interlayer d -spacing of $3.39\ \text{\AA}$. This change may indicate that the various oxygen containing functional groups as well as water molecules have been successfully removed during GO reduction and that RGO sheets have perfectly formed in the hybrid. The XRD patterns collected for ZnO and ZnO/RGO both show the same diffraction peaks at $2\theta=31.78^\circ, 34.48^\circ, 36.31^\circ, 47.61^\circ, 56.66^\circ, 62.94^\circ, 66.64^\circ,$ and 68.00° pertaining to the (100), (002), (101), (102), (110), (103), (200), (112), and (201) planes of ZnO, respectively, all of which are consistent with hexagonal phase wurtzite ZnO (JCPDS No. 36-1451) [19]. These results clearly

indicate that ZnO crystals had been successfully incorporated onto the RGO flakes.

The averaged crystallite size (thickness) is estimated using the FWHM (full width at half maximum) value of the XRD peaks and Scherrer's Eq. (1) [20,21]:

$$D = K \cdot \lambda / \beta \cdot \cos\theta \quad (1)$$

where D is the averaged crystallite size (thickness), λ is the incident wavelength, θ is the Bragg angle and β is the diffracted FWHM (radian). The averaged size of the ZnO NPs calculated using the value from the most intense peak were approximately $38.7\ \text{nm}$ for pure ZnO and $35.2\ \text{nm}$ for the hybrid samples. By fitting the (002) reflection in the pattern collected for the ZnO/RGO hybrid and again using the Scherrer formula ($N = \text{Thickness } (D) / d_{(002)}$), it is possible to estimate the average number of graphene layers (N) [21,22]. Based on the Scherrer equation the crystallite thickness (D) of RGO is estimated to be $1.7\ \text{nm}$ with an inter-planar spacing of $3.69\ \text{\AA}$. Thus we confirm the obtained composite is formed with $4\sim 5$ layers of reduced graphene sheets.

Raman spectra of pure ZnO and ZnO/RGO composite were also collected in order to characterize and compare the samples, and were shown in Fig. 3. For pure ZnO NPs three characteristic Raman bands are observed at $327\ (\text{E}_2^{\text{high}} - \text{E}_2^{\text{low}} \text{ mode})$, $437\ (\text{E}_2^{\text{high}} \text{ mode})$, and $605\ \text{cm}^{-1}\ (\text{E}_1(\text{LO}) \text{ mode})$ [15]. In the case of ZnO/RGO, an intense peak at $\sim 429\ \text{cm}^{-1}$ is seen and corresponds to the E_2^{high} mode for pure ZnO NPs. The other characteristic Raman bands in ZnO are found to be suppressed, indicating that ZnO in hybrid form is highly crystalline with a hexagonal wurtzite phase [15]. Both GO and the ZnO/RGO catalyst display a distinct G-band around $1595\ \text{cm}^{-1}$ ($1599\ \text{cm}^{-1}$ for GO and $1591\ \text{cm}^{-1}$ for ZnO/RGO) due to the E_{2g} vibrational mode of the sp^2 bonded carbon, as well as a D-band around $1350\ \text{cm}^{-1}$ ($1352\ \text{cm}^{-1}$ for GO and $1348\ \text{cm}^{-1}$ for ZnO/RGO) owing to the A_{1g} mode breathing vibrations of the six-membered sp^2 carbon rings. The G band shifting from $1599\ \text{cm}^{-1}$ to $1591\ \text{cm}^{-1}$ in GO vs. ZnO/RGO composite indicates that a distinct charge transfer exists between the graphitic structures and the oxygen related functional groups or ZnO NPs [23]. In addition, the ratio of D- vs. G-band intensity (I_D/I_G) for the ZnO/RGO hybrid (0.99) is higher than the ratio calculated for GO (0.91), a difference which may be attributed to the increased number of small sp^2 domains within the ZnO/RGO hybrid [8]. It has also been reported that the band intensity ratio, I_G/I_D , can be used to calculate the in plane crystallite size (L_a) using the equation $L_a = 19.0I_G/I_D - 19.0I_G/I_D$

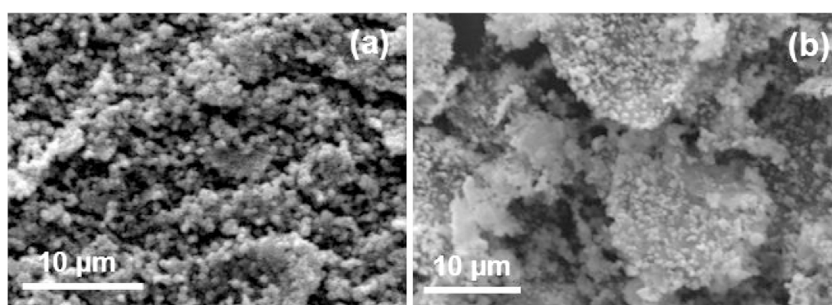


Fig. 1. XRD patterns of ZnO, GO and ZnO/RGO samples.

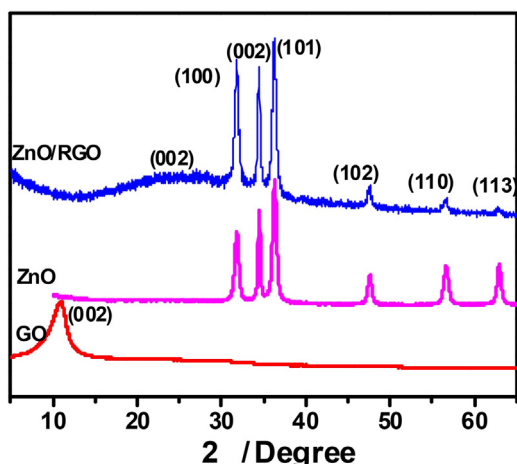


Fig. 2. SEM images of ZnO and ZnO/RGO samples.

[24]. According to I_G/I_D ratio of GO and ZnO/RGO in their Raman spectra, the in-plane crystallite sizes (L_a) of GO and ZnO/RGO are calculated to be 20.9 nm and 19.2 nm, respectively. This indicates that the functionalization and incorporation of ZnO NPs had barely any effect on the crystalline size of ZnO/RGO.

Evidence of the reduction of GO and incorporation of ZnO into the ZnO/RGO composite has also been observed using UV–vis and FT-IR spectrometry. The UV–vis absorption spectra collected for pure ZnO, GO, and ZnO-decorated RGO composites with their dispersions in ethanol are shown in Fig. 4. An absorption band at 227 nm in GO was assigned to the π - π^* transitions of aromatic C–C bonds [25] while the observed absorption peak at 276 nm for RGO is due to the π - π^* transitions in the graphitic structure. It is found that the difference is attributed to an increase in electronic conjugation in reduction form of GO [26,27]. The pure ZnO not only has a sharp UV absorption band at 368 nm that corresponds to the free excitonic absorption of ZnO particles [28], but also has weak visible light absorption that attributes either to chemical interactions induced defects in ZnO matrix or to narrowed band gap of ZnO that allows the absorption of longer-wavelength light or a combination of these effects [29]. The ZnO/RGO hybrid also displays the same sharp UV absorption peak, but it is redshifted slightly to 373 nm, suggesting a strong coupling effect between ZnO and graphene flakes. Also of note is the appearance of a new absorption peak at 213 nm for the ZnO/RGO hybrid, a feature most likely indicative of interactions between graphene and ZnO [11]. More importantly, ZnO/RGO composite shows an intense and

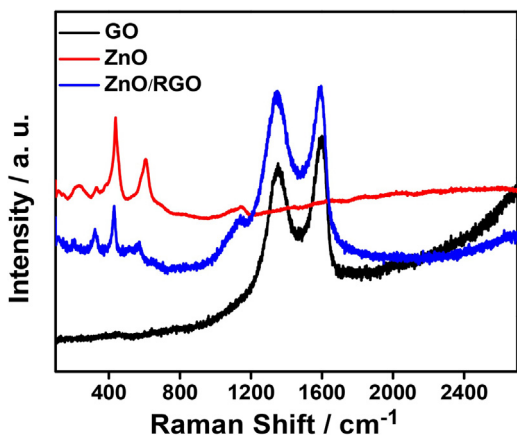


Fig. 3. Raman spectra of ZnO, GO and ZnO/RGO samples.

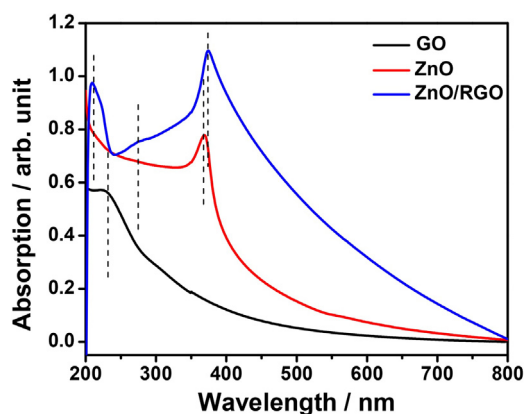


Fig. 4. UV–vis absorption spectra of ZnO, GO and ZnO/RGO samples.

broad background absorption across the entire visible region, as compared to pure ZnO which does not. All of these differences suggest the successful conversion of GO to RGO followed by incorporation of ZnO NPs onto the RGO flakes.

FT-IR spectra of ZnO, GO, and ZnO/RGO catalyst are shown in Fig. 5. The spectrum of GO (Fig. 5a) displays bands at 3452 cm^{-1} due to —OH stretching, 1746 cm^{-1} due to C=O stretching vibrations in the carboxylic acid, and 1626 cm^{-1} due to skeletal vibrations of unoxidized graphitic domains [30]. In the case of ZnO, a very clear absorption band is observed at 462.4 cm^{-1} due to the stretching vibration of Zn—O (Fig. 5b) [31,32,33]. As for the spectrum of ZnO/RGO (Fig. 5c), the characteristic peak corresponding to the C=C skeletal vibration is observed to shift to 1588 cm^{-1} from 1626 cm^{-1} in GO, which indicates chemical bondings of Zn—C or Zn—O—C between graphene flakes and ZnO [34]. Additionally, the absorption peaks due to the C=O stretching (1746 cm^{-1}) of COOH groups in GO have vanished, and the new bond appears around 1090 cm^{-1} due to the stretching vibration of the Zn—O—C bond, indicating chemical bonding of Zn atoms onto C=O groups of graphene oxide flakes [29,34,35]. Furthermore, the spectrum of ZnO/RGO appears the same bond around 462.6 cm^{-1} due to the stretching vibration of the Zn—O bond. The observed conformational changes that have appeared in the ZnO/RGO spectrum give further evidence of successful incorporation of ZnO onto the RGO flakes through covalent bonding as well as complete reduction of GO sheets to RGO sheets during in-situ synthesis. To further confirm and discern the chemical bonding between ZnO and graphene flakes in ZnO/RGO hybrid, XPS spectra of the O1s core level of ZnO/RGO hybrid has been measured and presented in Fig. S1. The de-convoluted high

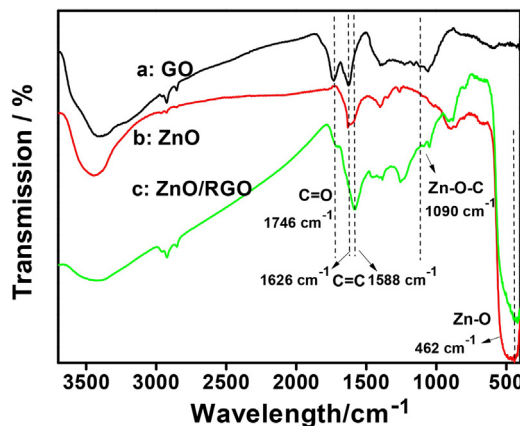


Fig. 5. FT-IR spectra of ZnO, GO and ZnO/RGO samples.

resolution O1 s spectra of ZnO/RGO hybrid consists of four peaks located at 530.9 eV, 531.5 eV, 532.4 eV, and 533.4 eV, which clearly correspond to O^{2-} in the wurtzite structure of ZnO lattice, O^{2-} defects with ZnO matrix, and chemically bonding of Zn atoms onto C=O, C–O functional groups of graphene flakes via Zn–O–C bond, respectively [29]. This result indicates that chemical bonding between ZnO and RGO flakes successfully occurs through Zn–O–C bonds during the in-situ synthesis process of ZnO/RGO hybrid, and agrees with our IR analysis well.

The charge separation and transfer abilities of a photocatalytic material determine, at least to some extent, its photocatalytic efficiency. In order to further understand the superior photocatalytic activity of the ZnO/RGO composite, transient photovoltaic (TPV) measurements are collected and analyzed. This method can be used to directly reflect the photo-induced charge carrier dynamics during pure ZnO and its hybrid, such as lifetime and transfer process of the electron-hole pairs. Such measurements are useful in order to clearly understand the mechanism of the photocatalytic processes in the present system. Fig. 6 shows the measured TPV curves of the ZnO and ZnO/RGO samples, both of which display distinct dynamic processes of photogenerated carrier. The pure ZnO crystal has very short carrier separation and slow transfer processes; while the ZnO/RGO hybrid has a relatively fast separation ratio and a long lifetime of photo-induced charge carrier. The lifetime of the photo-induced electron-hole pairs in pure ZnO NPs is about 10^{-6} – 10^{-7} sec, a much shorter lifetime is measured for the ZnO/RGO hybrid (10^{-6} – 10^{-3} sec). The intensity of the TPV response for ZnO is also much weaker than that measured for the ZnO/RGO hybrid. This indicates that there is both a large separation between the photogenerated electrons and holes occurring in the ZnO/RGO hybrid and efficient transfer of the photogenerated electrons to the RGO sheets [16]. This means that electron-hole pair recombination is quenched in the composite material. The availability of electrons in the material hints that they may be available for pollutant degradation, a question that is discussed in the following paragraphs.

The photocatalytic degradation efficiency of pure ZnO and ZnO/RGO hybrid is evaluated onto RhB dye in water with concentration of 2×10^{-2} mg/ml. Sample solutions are exposed to UV light irradiation and the remaining dye is measured using UV-vis spectrometry. Fig. 7 shows that with 55 min of irradiation, ZnO/RGO hybrid, ZnO-RGO mixture and ZnO degrade 100%, 61% and 80% of the dye, respectively. It is found that the ZnO/RGO hybrid shows enhanced activity compared to pure ZnO and ZnO-RGO mixture with simple mixing. Here, the distinct photocatalytic efficiency between ZnO/RGO hybrid and ZnO-RGO mixture has also verified the chemical bonding through Zn–O–C bonds during ZnO/RGO

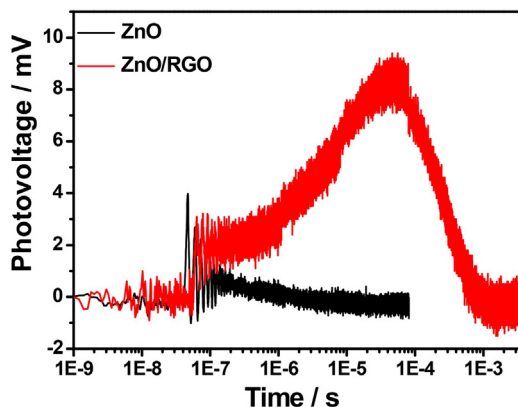


Fig. 6. Surface photovoltage spectra of ZnO crystals and ZnO/RGO samples.

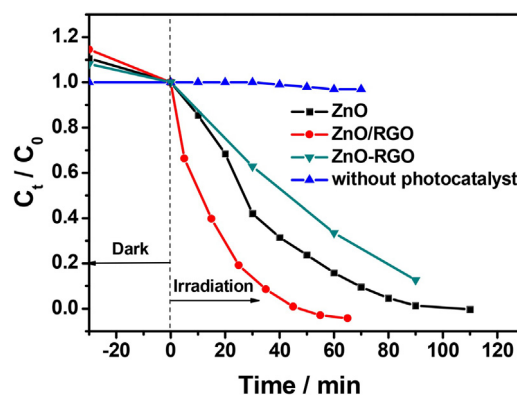


Fig. 7. Photocatalytic degradation spectra of RhB over photocatalyst-free solution, ZnO crystals, ZnO-RGO mixture and ZnO/RGO hybrid.

hybrid plays a great role in promoting the photocatalytic process of dyes in profile.

The apparent rate constant for the photodegradation of RhB dye is calculated using the following equation: $k = \ln(C_t/C_0)$ [8], as displayed in Fig. 8. The average value of the apparent rate constant for ZnO/RGO composites is $k = 0.095 \text{ min}^{-1}$, a value 2.2 times higher than that measured for pure ZnO NPs ($k = 0.043 \text{ min}^{-1}$). Based on these results it is obvious that the photocatalytic reactivity of ZnO/RGO is greater than that of ZnO NPs. Generally, a photocatalyst should have highly catalytic reproducibility in cyclic application. To test the photocatalytic reproducibility of the ZnO/RGO hybrid three cycles of photodegradation experiment of contaminant RhB are carried out. As shown in Fig. 9, RhB is totally decomposed during each cycle, and the reduction in reproducible photoactivities of ZnO/RGO hybrid is much slow: 60 min for the first recycle, 70 min for the second, and 75 min for the third. This efficient photocatalytic activity and reproducibility of the ZnO/RGO hybrid mean that it has potential as a photocatalyst for practical applications.

The photodegradation process of organic dyes through ZnO/RGO hybrid catalyst under full range of sunlight irradiation could involve both excitation of ZnO semiconductor and dye molecules [9,10]. Dye molecules are easily adsorbed onto graphene sheets due to π - π stacking between graphene and conjugated dye molecules [9]. Solar-wave light irradiation leads to the excitation of ZnO crystals and dye molecules and induces the generation of electrons. This step is followed by electron transfer from the excited dye (dye*) to RGO or from the conduction band of ZnO and then to RGO [9,10], which may subsequently generate massive reactive oxygen species (ROs) that oxidize the dye compounds [10]. As it reported

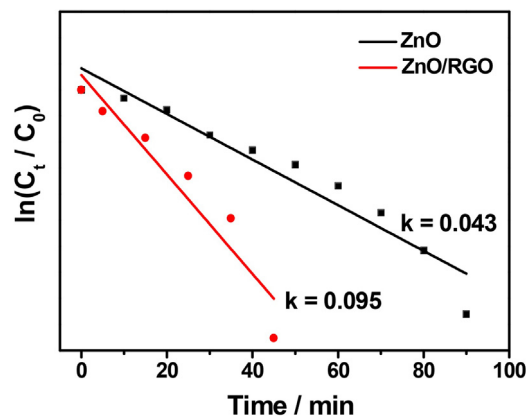


Fig. 8. Kinetic linear simulation curves of photocatalytic degradation of RhB over ZnO crystals and ZnO/RGO hybrid.

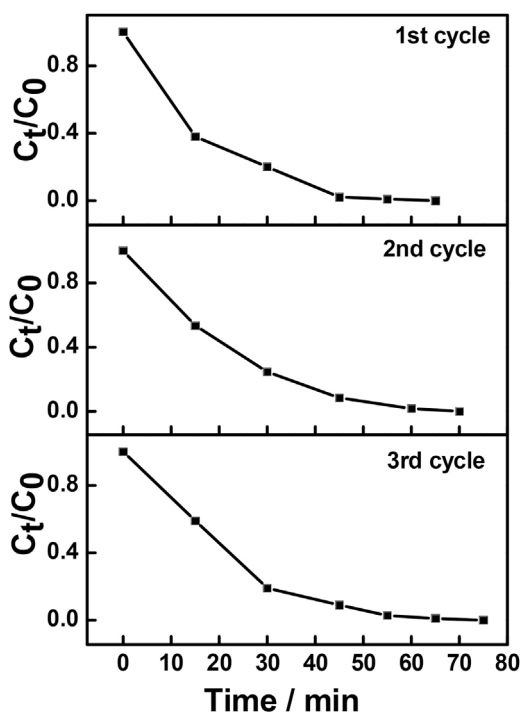


Fig. 9. Cycling runs in photocatalytic degradation of RhB in presence of ZnO/RGO hybrid.

ZnO crystals have the potential of the conduction band (-4.05 eV) and the valence band (-7.25 eV) as well as that of graphene (-4.42 eV) [10,35], it is reasonable that excited electrons from the RhB dye under visible light region should directly transfer from the RhB dye* to the graphene flakes. However, on the one hand, for our present system under visible light irradiation using a 300 W Xe light fixed with a 400 nm cutoff filter, RhB dye molecules can not degrade even if RhB dye molecules have characteristic absorption peak around 554 nm in the visible light region. The absorption intensity of RhB did not show any obvious decrease in the absorption wavelength with increasing irradiation time. (see Fig. S2) On the other hand, for our present system under ultraviolet region, the electrons can be effectively excited and quickly derived from ZnO crystals to RGO, which is regarded as an effective and rapid electron acceptor due to covalent Zn–O–C bonding between ZnO and RGO flakes during in-situ synthesized process, for lengthening the life time of the excited electrons [9,10,38], confirmed by the TPV spectra without H_2O_2 . These separated electrons combine with surface oxygen, and then generate a series of active oxygen radicals such as $O_2^{\cdot-}$ [9,10,36,37]. The generated free radicals can further act as active species to react with the nearby dye molecules and facilitate complete degradation. These controlled experiments provided evidence that the degradation of RhB is not due to the excitation of RhB but to the excitation of the ZnO/RGO. In this way effective electron separation and quick electron transfer are responsible for the enhanced photocatalytic performance of the ZnO/RGO hybrid.

4. Conclusion

A hybrid catalyst of ZnO crystals covalently modified few-layered RGO flakes has been successfully synthesized in-situ using a facile solution procedure requiring only zinc acetate as a ZnO precursor and DMF as a reduction reagent for GO. A series of

morphology and structural characterization studies including: SEM, XRD, Raman, FT-IR, XPS, and UV-vis spectroscopy, have shown that ZnO crystals are strongly attached onto a few-layered RGO flakes through covalent Zn–O–C bonding, even when considering ultrasonic influence. This result is further confirmed by its reproducible photocatalytic activity during three consecutive uses. The ZnO/RGO hybrid has exhibited higher photocatalytic activity and reproducible catalytic stability than pure ZnO. The photodegradation efficiency of 2×10^{-2} mg/ml RhB is 100% in 55 min when using a small amount (0.15 mg/ml) of the ZnO/RGO composite. The catalytic activity still achieves a 100% degradation ratio of RhB after 75 min in spite of the third consecutive use. This is mainly due to the highly effective electron transfer path between ZnO and RGO flakes through in-situ reaction induced covalent bonding. The measured TPV results for ZnO/RGO clearly validate that photoelectron-hole pair recombination has been reduced as well as the lifetimes for photo-generated electrons transferring to graphene flakes from the surface of the ZnO have been improved. The assembly of ZnO crystals covalently linking with few-layered graphene flakes is responsible for the enhanced activity of the ZnO/RGO composite compared to ZnO, and is beneficial for photocatalytic reproducibility in cyclic practical application.

Acknowledgments

This research was partially supported by the National Nature Science Foundation of China (61605167), the Science and Technology Research Project (172102310478, 162102410093) of Henan Province, and Plan for Scientific Innovation Talent of Henan Province (174100510014). Prof. SH Lee would like to thank supports by the selection of research-oriented professor of Chonbuk National University in 2017.

Appendix A. Supplementary data

Supplementary data associated with this article can be found, in the online version, at <http://dx.doi.org/10.1016/j.jphotochem.2017.08.005>.

References

- [1] M.R. Hoffmann, S.T. Martin, W.Y. Choi, D.W. Bahnemann, Bahnemann Environmental applications of semiconductor photocatalysis, *Chem. Rev.* 95 (1995) 69–96.
- [2] M. Miyachi, A. Nakajima, T. Watanabe, K. Hashimoto, Photocatalysis and photoinduced hydrophilicity of various metal oxide thin films, *Chem. Mater.* 14 (2002) 2812–2816.
- [3] G. Rani, P.D. Sahare, Structural and spectroscopic characterizations of ZnO quantum dots annealed at different temperatures, *J. Mater. Sci. Technol.* 29 (2013) 1035–1039.
- [4] O. Yayapao, T. Thongtem, A. Phuruangrat, S. Thongtem, Ultrasonic-assisted synthesis of Nd-doped ZnO for photocatalysis, *Mater. Lett.* 90 (2013) 83–86.
- [5] A. McLaren, T. Valdes-Solis, G.Q. Li, S.C. Tsang, Shape and size effects of ZnO nanocrystals on photocatalytic activity, *J. Am. Chem. Soc.* 131 (2009) 12540–12541.
- [6] Y.F. Chen, C.J. Zhang, W.X. Huang, Y. Situ, H. Huang, Multimorphologies nano-ZnO preparing through a simple solvothermal method for photocatalytic application, *Mater. Lett.* 141 (2015) 294–297.
- [7] C.S. Chen, T.G. Liu, L.W. Lin, X.D. Xie, X.H. Chen, Q.C. Liu, B. Liang, W.W. Yu, C.Y. Qiu, Multi-walled carbon nanotube-supported metal-doped ZnO nanoparticles and their photocatalytic property, *J. Nanopart. Res.* 15 (2013) 1295–1303.
- [8] R.T. Thomas, P.A. Rasheed, N. Sandhyarani, Synthesis of nanotitania decorated few-layer graphene for enhanced visible light driven photocatalysis, *J. Colloid Interface Sci.* 428 (2014) 214–221.
- [9] B.X. Li, T.X. Liu, Y.F. Wang, Z.F. Wang, ZnO/graphene-oxide nanocomposite with remarkably enhanced visible-light-driven photocatalytic performance, *J. Colloid Interface. Sci.* 377 (2012) 114–121.
- [10] B.J. Li, H.Q. Cao, ZnO@graphene composite with enhanced performance for the removal of dye from water, *J. Mater. Chem.* 21 (2011) 3346–3349.
- [11] J.L. Wu, X.Q. Shen, L. Jiang, K. Wang, K.M. Chen, Solvothermal synthesis and characterization of sandwich-like graphene/ZnO Nanocomposites, *Appl. Sur. Sci.* 256 (2010) 2826–2830.

- [12] G.M. Neelgund, A. Oki, Z.P. Luo, ZnO and cobalt phthalocyanine hybridized graphene: efficient photocatalysts for degradation of rhodamine B, *J. Colloid Interface Sci.* 430 (2014) 257–264.
- [13] A. Cao, Z. Liu, S.S. Chu, M.H. Wu, Z.M. Ye, Z.W. Cai, Y.L. Chang, S.F. Wang, Q.H. Gong, Y.F. Liu, A facile one-step method to produce graphene-CdS quantum dot nanocomposites as promising optoelectronic materials, *Adv. Mater.* 22 (2010) 103–106.
- [14] J.F. Wang, T. Tsuzuki, B. Tang, X.L. Hou, L. Sun, X.G. Wang, Reduced graphene oxide/ZnO composite: reusable adsorbent for pollutant management, *Appl. Mater. Inter.* 4 (2012) 3084–3090.
- [15] F.T. Johra, W.G. Jung, RGO-TiO₂-ZnO composites: synthesis, characterization, and application to photocatalysis, *Appl. Catal. A: Gen.* 491 (2015) 52–57.
- [16] W.W. Tie, S.S. Bhattacharyya, Y.J. Lim, S.W. Lee, T.H. Lee, S.H. Lee, et al., Dynamic electro-optic response of graphene/graphitic flakes in nematic liquid crystals, *Opt. Express* 21 (2013) 19867–19879.
- [17] W.S. Hummers, R.E. Offeman, Preparation of graphitic oxide, *J. Am. Chem. Soc.* 80 (1958) 1339.
- [18] Y. Lei, L.Y. Gu, W.W. He, Z.X. Jia, X.G. Yang, H.M. Jia, Z. Zheng, Intrinsic charge carrier dynamics and device stability of perovskite/ZnO mesostructured solar cells in moisture, *J. Mater. Chem. A* 4 (2016) 5474–5481.
- [19] D.I. Son, B.W. Kwon, D.H. Park, W.S. Seo, Y.J. Yi, B. Angadi, C.-L. Lee, W.K. Choi, Emissive ZnO-graphene quantum dots for white-light-emitting diodes, *Nat. Nanotechnol.* 7 (2012) 465–471.
- [20] P. Bindu, S. Thomas, Estimation of lattice strain in ZnO nanoparticles: x-ray peak profile analysis, *J. Theor. Appl. Phys.* 8 (2014) 123–134.
- [21] K.S. Subrahmanyam, S.R.C. Vivekchand, A. Govindaraj, C.N.R. Rao, A study of graphenes prepared by different methods: characterization, properties and solubilization, *J. Mater. Chem.* 18 (2008) 1517–1523.
- [22] H.M. Ju, S.H. Huh, S. Choi, H. Lee, Structures of thermally and chemically reduced graphene, *Mater. Lett.* 64 (2010) 357–360.
- [23] M.H. Jin, H.K. Jeong, T.H. Kim, K.P. So, Y. Cui, W.J. Yu, E.J. Ra, Y.H. Lee, Synthesis and systematic characterization of functionalized graphene sheets generated by thermal exfoliation at low temperature, *J. Phys. D: Appl. Phys.* 43 (2010) 275402.
- [24] M.A. Pimenta, G. Dresselhaus, M.S. Dresselhaus, L.A. Cancado, A. Jorio, R. Sato, Studying disorder in graphite-based systems by Raman spectroscopy, *Phys. Chem. Chem. Phys.* 9 (2007) 1276–1290.
- [25] J.I. Paredes, S. Villar-Rodil, A. Marti'nez-Alonso, J.M.D. Tasco'n, Graphene oxide dispersions in organic solvents, *Langmuir* 24 (2008) 10560–10564.
- [26] Y. Zhou, Q.L. Bao, L.A.L. Tang, Y.L. Zhong, K.P. Loh, Hydrothermal dehydration for the Green reduction of exfoliated graphene oxide to graphene and demonstration of tunable optical limiting properties, *Chem. Mater.* 21 (2009) 2950–2956.
- [27] K. Krishnamoorthy, G.S. Kim, S.J. Kim, Graphene nanosheets: ultrasound assisted synthesis and characterization, *Ultrason. Sonochem.* 20 (2013) 644–649.
- [28] X.M. Ho, ZnO/Ag heterostructured nanoassemblies: wet-chemical preparation and improved visible-light photocatalytic performance, *Mater. Lett.* 139 (2015) 201–204.
- [29] M.M. Hossain, B.-C. Ku, J.R. Hahn, Synthesis of an efficient white-light photocatalyst composite of graphene and ZnO nanoparticles: application to methylene blue dyedecomposition, *Appl. Surf. Sci.* 353 (2015) 55–65.
- [30] D.Y. Liang, C. Cui, H.H. Hu, Y.P. Wang, S. Xu, B.L. Ying, P.G. Li, B.Q. Lu, H.L. Shen, One-step hydrothermal synthesis of anatase TiO₂/reduced graphene oxide nanocomposites with enhanced photocatalytic activity, *J. Alloy. Com.* 582 (2014) 236–240.
- [31] R.Y. Hong, J.H. Li, L.L. Chen, D.Q. Liu, H.Z. Li, Y. Zheng, J. Ding, Synthesis, surface modification and photocatalytic property of ZnO nanoparticles, *Powder Technol.* 189 (2009) 426–432.
- [32] V. Srikant, D.R. Clarke, On the optical band gap of zinc oxide, *J. Appl. Phys.* 83 (1998) 5447–5451.
- [33] H.F. Lin, S.C. Liao, S.W. Hung, The dc thermal plasma synthesis of ZnO nanoparticles for visible-light photocatalyst, *J. Photochem. Photobiol. A* 174 (2005) 82–87.
- [34] M. Samadi, H.A. Shivaee, M. Zanetti, A. Pourjavadi, A. Moshfegh, Visible light photocatalytic activity of novel MWCNT-doped ZnO electrospun nanofibers, *J. Mol. Catal. A* 359 (2012) 42–48.
- [35] J.Y. Chen, H.M. Zhang, P. Liu, Y.B. Li, X.L. Liu, G.Y. Li, P.K. Wong, T.C. An, H.J. Zhao, Cross-linked ZnIn₂S₄/rGO composite photocatalyst for sunlight-driven photocatalytic degradation of 4-nitrophenol, *Appl. Catal. B: Environ.* 168–169 (2015) 266–273.
- [36] M. Sadeghi, W. Liu, T.G. Zhang, P. Stavropoulos, B. Levy, Role of photoinduced charge carrier separation distance in heterogeneous photocatalysis: oxidative degradation of CH₃OH vapor in contact with Pt/TiO₂ and cofumed TiO₂/Fe₂O₃, *J. Phys. Chem.* 100 (1996) 19466–19474.
- [37] D.J. Yang, H.W. Liu, Z.F. Zheng, Y. Yuan, J.C. Zhao, E.R. Waclawik, X.B. Ke, H.Y. Zhu, An efficient photocatalyst structure: tiO₂(B) nanofibers with a shell of anatase nanocrystals, *J. Am. Chem. Soc.* 131 (2009) 17885–17893.
- [38] R. Thankam Thomas, P. Abdul Rasheed, N. Sandhyarani, Synthesis of nanotitania decorated few layer graphene for enhanced visible light driven photocatalysis, *J. Colloid Interface Sci.* 428 (2014) 214–221.